ADVANCED FUNCTIONAL MATERIALS
www.afm-journal.de

MoS_2 Formed on Mesoporous Graphene as a Highly Active Catalyst for Hydrogen Evolution

*Lei Liao, Jie Zhu, Xiaojun Bian, Lina Zhu, Micheál D. Scanlon, Hubert H. Girault, and Baohong Liu**

A highly active and stable electrocatalyst for hydrogen evolution is developed based on the in situ formation of MoS_2 nanoparticles on mesoporous graphene foams (MoS_2/MGF). Taking advantage of its high specific surface area and its interconnected conductive graphene skeleton, MGF provides a favorable microenvironment for the growth of highly dispersed MoS_2 nanoparticles while allowing rapid charge transfer kinetics. The MoS_2/MGF nanocomposites exhibit an excellent electrocatalytic activity for the hydrogen evolution reaction with a low overpotential and substantial apparent current densities. Such enhanced catalytic activity stems from the abundance of catalytic edge sites, the increase of electrochemically accessible surface area and the unique synergic effects between the MGF support and active catalyst. The electrode reactions are characterized by electrochemical impedance spectroscopy. A Tafel slope of ≈42 mV per decade is measured for a MoS_2/MGF modified electrode, suggesting the Volmer-Heyrovsky mechanism of hydrogen evolution.

1. Introduction

Advanced materials for electrocatalytic and photo-electrochemical water splitting are central to the area of renewable energy. Developing new methods and materials for the conversion and storage of renewable energy sources, for example solar or wind, is a scientific grand challenge facing the world in the coming century. Central to this challenge is the proposed use of hydrogen as a major energy carrier.[1,2] Recently, sustainable hydrogen production from water splitting has attracted growing attention.[3–6] The electrochemical hydrogen evolution reaction (HER, i.e., $2H^+ + 2e^- \rightarrow H_2$) requires advanced catalysts with a high current density at a low overpotential. The most effective HER electrocatalysts in acidic media are those of Pt and its composites.[7–9] However, the large-scale application of Pt-type catalysts is limited due to their high cost and low-abundance. Therefore, the development of new advanced HER electrocatalysts, especially those composed of inexpensive and abundant materials, is crucial.

In recent years, molybdenum sulfide nanoparticles, capable of accepting electrons and protons, were highlighted as promising hydrogen evolution catalysts.[5,6,10–14] Nørskov's group calculated MoS_2's hydrogen binding energy and found it to be similar to that of Pt's.[15,16] MoS_2 reduces protons at low overpotentionals with a high current density and a quantitative current efficiency through its co-ordinated sulfur edge sites, while its basal planes remain catalytically inert.[15,17] As a result, nanosized MoS_2 is much more active than the relatively inert bulk form due to the presence of more exposed sulfur edge sites.[5,15,17,18] Development of catalysts with high activity and stability will be the ultimate objective. The catalysts morphology and electrical conductivity are the two key factors that influence electrocatalytic efficiency.[5,18] Taking these factors into account, carbon materials are ideal supports to improve the electrocatalytic activity because of their unique physicochemical properties. Recently, our group developed nanostructured MoS_2 on a mesoporous carbon material.[19] Strong chemical coupling and interactions between Mo precursors and functional mesoporous carbon nanospheres (MCNs) allowed the selective growth of highly dispersed MoS_2 nanoparticles (i.e., edge rich) on the MCNs (MoS_2/MCNs).[19] Leite and coworkers reported that graphene oxide was a highly selective substrate to synthesize a layered MoS_2 hybrid electrocatalyst.[20] Dai's group has synthesised MoS_2 on reduced graphene oxide sheets (MoS_2/GO) and demonstrated high HER electrocatalytic activity at a low overpotential and with small Tafel slopes.[21] Such findings implicitly indicate the significant potential of graphene in electrocatalysis.

Graphene with three-dimensional architectures has garnered increased attention recently from the fields of environmental research, sensors and biology.[22–24] Nanoporous graphene foams with controlled pore sizes at nanoscales were firstly prepared by Zhao and co-authors.[25] Such 3D structures not only prevent graphene sheets from restacking but also provide graphene materials with a high specific surface area, an

L. Liao, J. Zhu, X. Bian, L. Zhu, Prof. B. H. Liu
Department of Chemistry
State Key Lab of Molecular Engineering of Polymers and Institute of Biomedical Sciences
Fudan University, Shanghai 200433, China
E-mail: bhliu@fudan.edu.cn
Dr. M. D. Scanlon, Prof. H. H. Girault
Laboratoire d'Electrochemie Physique et Analytique
École Polytechnique Fédérale de Lausanne
CH-1015 Lausanne, Switzerland

DOI: 10.1002/adfm.201300318

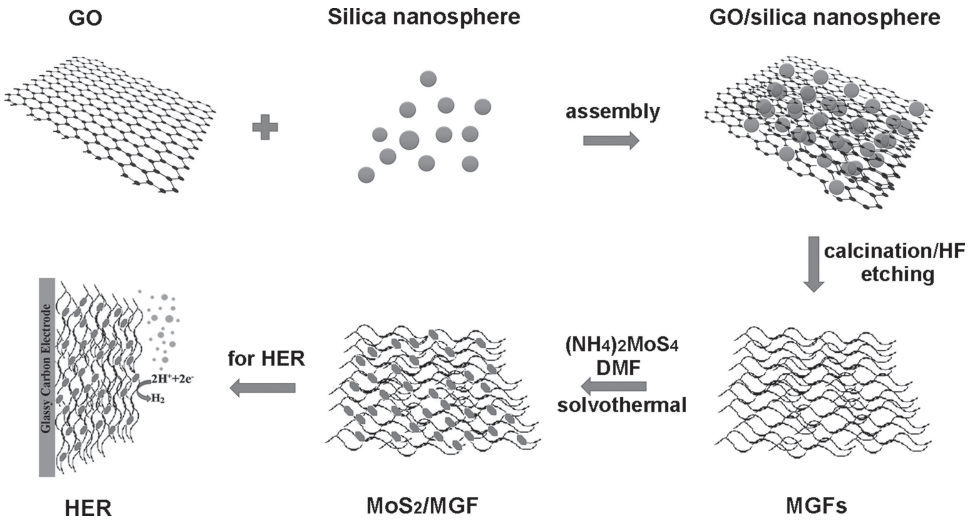

Scheme 1. Illustration of the synthesis procedures of MoS_2/MGF using as an electrocatalyst for hydrogen evolution reaction.

interconnected conductive network and a specific microenviroment due to the combination of a porous structure with the excellent intrinsic properties of graphene.[26,27] It is anticipated that nanoporous graphene as a loading matrix would enhance the activity of embedded electrocatalysts. Thus far, the HER catalysed by such a composite material has not been reported.

In this work, we developed an active catalyst nanocomposite of MoS_2 via an in situ hydrothermal route on a 3D architectural graphene, mesoporous graphene foam (MGF), with a nanometer scale pore size (**Scheme 1**). The 3D architectural graphene allowed the intimate growth of highly dispersed and ultrafine MoS_2 nanoparticles onto its surfaces, free of aggregation. Benefiting from its high specific surface area, adjustable mesopores and electrical conductivity, this MoS_2/MGF nanocomposite has been demonstrated to be the most active nonprecious metal material for electrochemical hydrogen evolution exhibiting low overpotential and high current densities.

2. Results and Discussion

2.1. Characterization of MoS_2/MGF Nanocomposites

Mesoporous graphene foams were prepared by using methyl group grafted silica nanospheres with a uniform size of ≈24.5 nm as the templates.[25,28] **Figure 1**A shows the transmission electron microscopy (TEM) image of silica spheres and their diameter distribution (insert). Graphene oxide sheets were employed as the precursor for the construction of MGF. In the TEM image (Figure 1B), both the porous structure and the flat layer could be observed. The N_2 adsorption-desorption plot and pore size distribution (Supporting Information, Figure S1; Figure 1B, insert) showed that MGF had a high surface area of 819 m^2 g^{-1} and a pore size of ≈25 nm, quite close to the particle diameter of the silica spheres, indicating that the pores were generated by the silica templates. MoS_2/MGF nanocomposites were prepared by a simple hydrothermal reaction of $(NH_4)_2MoS_4$ with hydrazine in DMF solution containing MGF as the matrix at 200 °C.[19,21] During this process, the $(NH_4)_2MoS_4$ precursor was reduced in situ to MoS_2 onto MGF matrices. The TEM image (Figure 1C) revealed that the highly dispersed and ultrafine MoS_2 nanoparticles (≈2 nm) were intimately grown on the graphene surfaces using MGFs as nucleation sites, thus massively increasing the catalytic edge sites in comparison to pure MoS_2 which was freely grown in solution where the particles aggregated into various sizes (Supporting Information, Figure S2). High-resolution TEM (HR-TEM) images showed hexagonal atomic lattices in the basal planes and abundant exposed edges of the MoS_2 nanoparticles (Figure 1D).[21] The drastic morphological differences highlight the important role of MGF as a novel support for mediating the growth of nanosized MoS_2. The nitrogen adsorption-desorption isotherm of MoS_2/MGF and pore size distribution (Supporting Information, Figure S3) showed that the hybrid MoS_2/MGF nanocomposite had the mesopore size of ≈20.6 nm. MGFs central attributes of a high surface area with abundant mesopores, in combination with the highly conducting skeleton of graphene allows MGF not only to facilitate the access of electrolyte, thus enabling the rapid diffusion of ions and electrons, but also to prevent the aggregation of graphene sheets and catalysts.

X-ray photoelectron spectroscopy (XPS) (**Figure 2**) was used to further confirm the thermal reduction of Mo (VI) to Mo (IV). The atomic percentages of Mo and S are 5.49% and 10.37%, respectively, and quite consistent with the theoretical values in MoS_2. The well defined spin-coupled Mo and S doublets, highlighted in Figures 2C,D, are nearly the same binding energies as those of commercial MoS_2 nanoparticles.[5,19,23] Two peaks are observed at approximately 228.9 eV and 232.3 eV, which can be attributed to Mo 3d 5/2 and Mo 3d 3/2 binding energies, respectively. In Figure 2D, the peaks at about 161.9 eV and 163.7 eV are related to S 2p 3/2 and S 2p 1/2 binding energies, respectively.

2.2. HER Electrocatalytic Activities of MoS_2/MGF Modified Electrodes

The electrocatalytic HER activities of MoS_2/MGF nanocomposites were investigated in 0.5 m H_2SO_4 solution by linear sweep voltammetry (LSV) using a three-electrode setup. The

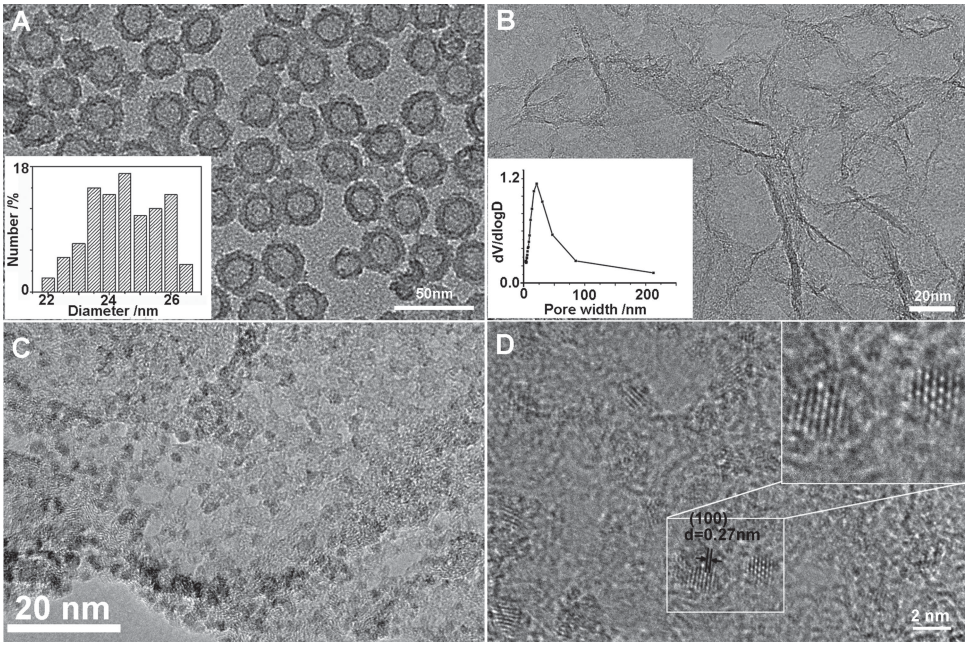

Figure 1. A) TEM image and diameter distribution (insert) of silica nanospheres. B) The TEM image and pore size distribution (insert) of mesoporous graphene foam (MGF). C) TEM image of MoS_2/MGF. D) High resolution TEM images of MoS_2/MGF. The insert shows a magnified image of the exposed edges of MoS_2 nanoparticles on MGF.

catalysts were deposited on a glassy carbon electrode (GCE) with a hybrid catalyst loading of 0.21 mg cm^{-2}. The area of the coated electrodes may exceed that of the glassy carbon disc, but we calculate all the current densities using the geometric value. **Figure 3**A depicts the polarization curves (*i-V* plot) for the different GCEs modified with MoS_2/MGF, free MoS_2 particles,

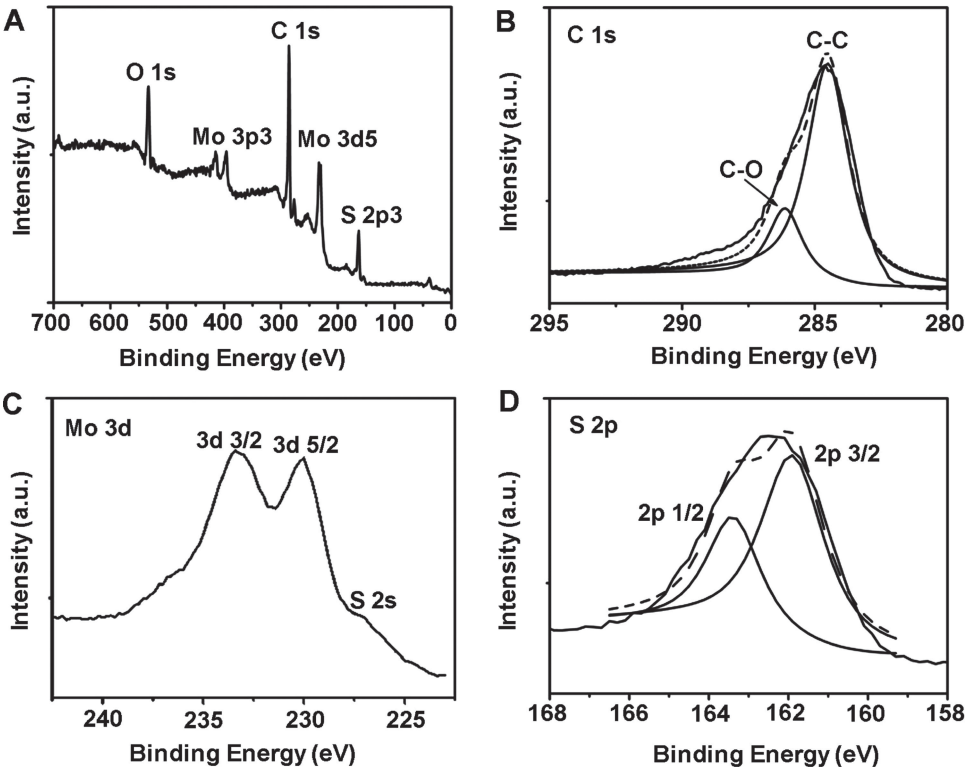

Figure 2. XPS of MoS_2/MGF nanocomposite. A) Survey spectrum. B) C 1s spectrum. C) Mo 3d spectrum. D) S 2p spectrum. The atomic percentage was determined to be Mo 5.49% and S 10.37%.

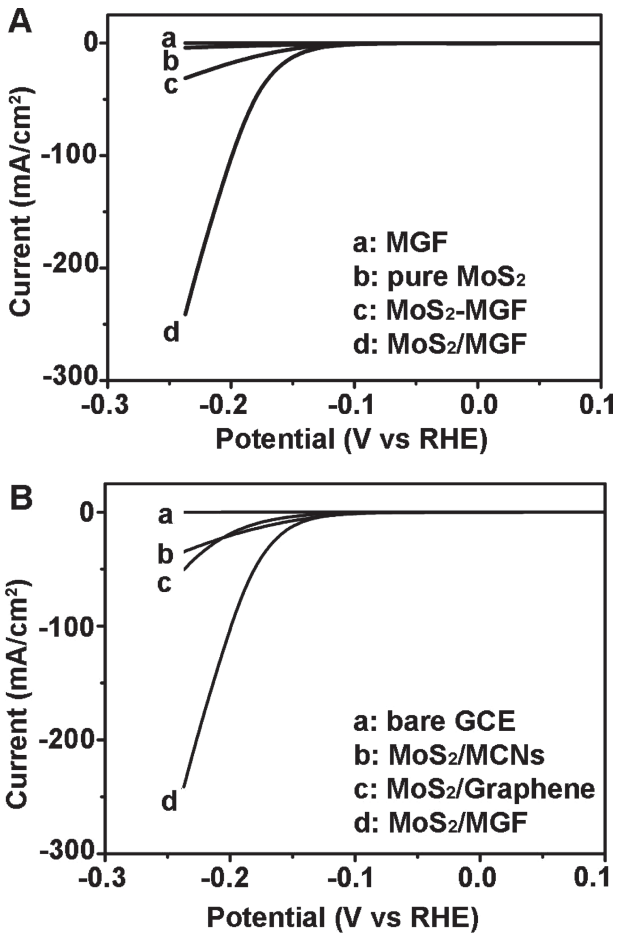

Figure 3. A) LSV polarization curves for glassy carbon electrodes modified with (a) MGF, (b) pure MoS_2, (c) MoS_2 physically mixed with MGFs (MoS_2-MGF), and (d) MoS_2-formed on MGFs (MoS_2/MGF) in 0.5 m H_2SO_4 at room temperature with a hybrid catalyst loading of 0.21 mg cm^{-2}. B) LSV polarization curves for (a) the bare glassy carbon electrode and the glassy carbon electrodes modified with (b) MoS_2-formed on mesoporous carbons (MoS_2/MCNs), (c) MoS_2 formed on graphene sheets (MoS_2/graphene) and (d) MoS_2/MGF in 0.5 m H_2SO_4 with a hybrid catalyst loading of 0.21 mg cm^{-2}. Scan rate: 2 mV s^{-1}.

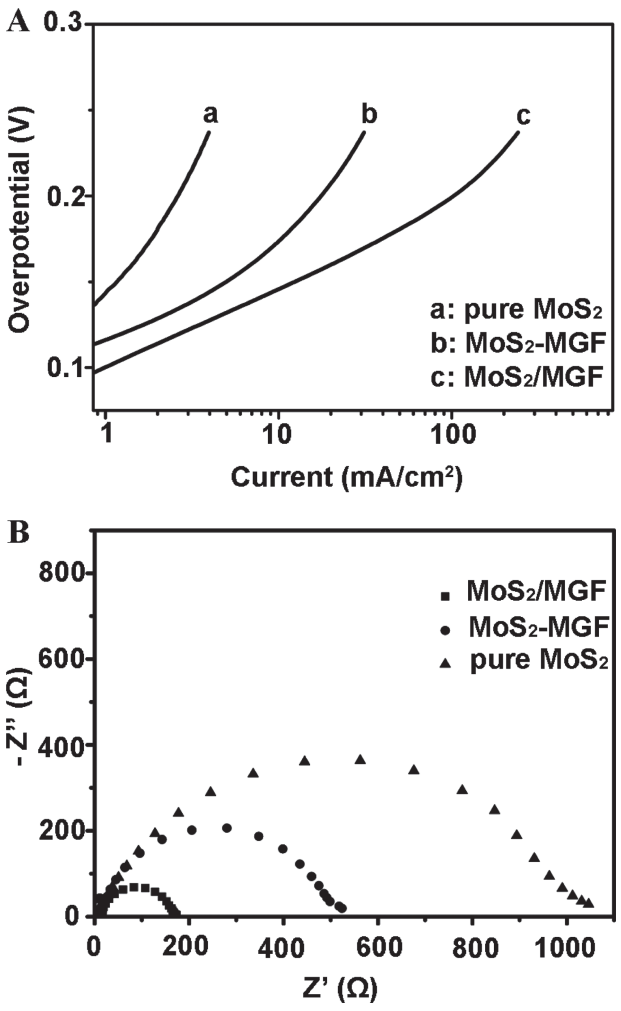

Figure 4. A) Tafel plots recorded on the corresponding electrodes and B) electrochemical impedance spectra of electrodes modified with MoS_2/MGF, MoS_2 physically mixed with MGF (MoS_2-MGF) and pure MoS_2 particles.

free MGF, a physical mixture of MoS_2 and MGFs (MoS_2-MGF), respectively. The polarization curve recorded by the as-prepared MoS_2/MGF-GCE showed a small overpotential (h) of ≈100 mV for the HER with substantial apparent current densities (j) of ≈100 mA cm^{-2} at h = 200 mV, relative to the geometric area of the electrode. In contrast, either free MoS_2 particles or a physical mixture of MoS_2 and MGFs exhibited little HER catalytic activity in terms of the onset potential and current densities, while a MGF modified GCE showed no catalytic activity in the absence of MoS_2 (Figure 3A). Though a small overpotential of ≈100 mV for the HER was also observed for MoS_2/graphene and MoS_2/mesoporous carbon prepared by the same method, their catalytic current densities were about ca. 30–40 mA cm^{-2} at h = 200 mV, respectively (Figure 3B). To further emphasize the importance of both mesopores and the conductivity of graphene in order to achieve a higher HER activity, control experiments were carried out for GCEs modified with MoS_2 on non-porous graphene (without SiO_2 nanosphere as a template) from high temperature annealing (Supporting Information, Figure S4). The polarization curves showed that the catalytic current density of MoS_2/non-porous graphene was higher than that of MoS_2/graphene without high temperature treatment, but lower than that of MoS_2/MGF. These results indicate that both the conductive graphene skeleton and mesopores of MGF are important to enhance the electrocatalytical activity of MoS_2/MGF for the HER.

The linear portions of the Tafel plots were fitted to the Tafel equation (h = b log j + a, where j is the current density and b is the Tafel slope), yielding Tafel slopes of ≈42 mV $decade^{-1}$ (h = 90–120 mV) and ≈85 mV $decade^{-1}$ (h = 110–130 mV) for MoS_2/MGF nanocomposites and free MoS_2 particles, respectively (**Figure 4**A). The significantly improved electrocatalysis exhibited by the MoS_2/MGF-modified GCE suggests a smaller activation energy for the HER or may be directly attributed to optimisation of the specific amount of catalytic edge sites on the electrode surface for the nanocomposite. MoS_2 nanoparticles

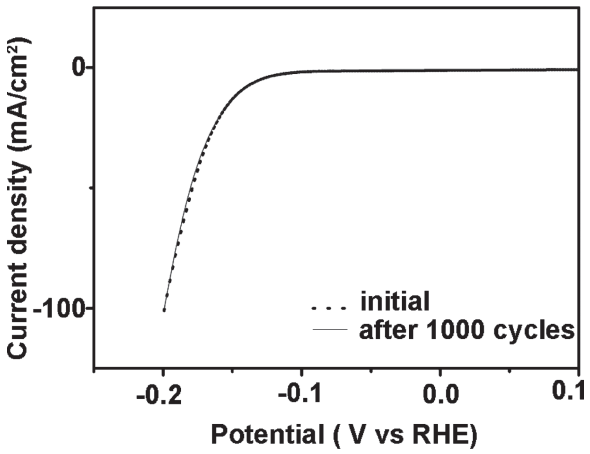

Figure 5. Stability for the MoS_2/MGF modified electrode with initial LSV polarization curve (dotted) and after 1000 cycles (line) in 0.5 m H_2SO_4 with a hybrid catalyst loading of 0.21 mg cm^{-2} and scan rate of 10 mV s^{-1}.

grown on MGF are confined such that very small, dispersed and thereby edge-rich MoS_2 is formed, while the graphene network supplies excellent electronic conductivity. The optimal activity of the MoS_2/MGF catalyst may also be attributed to strong chemical and electronic coupling between the MGF and MoS_2, permitting highly efficient electrical communication between the catalytic edge sites and the underlying electrode substrate. This hypothesis was further confirmed by impedance measurements in 0.5 m H_2SO_4 (Figure 4B). The MoS_2/MGF-modified GCE displayed much lower impedance than GCEs modified either by pure MoS_2 particles or a physical mixture of MoS_2 and MGF, similar to that of a MoS_2/GO modified GCE.[21] Thus, much faster electron transfer between the catalytic edge sites of MoS_2/MGF and the electrode substrate is one of the key factors contributing to the superior HER kinetics. The catalytic stability of the MoS_2/MGF catalyst towards the HER was assessed. Polarization curves of MoS_2/MGF-modified electrode were carried out continuously in 0.5 m H_2SO_4. After 1000 cycles, the catalyst showed similar *i-V* curves with negligible decay of cathodic currents (**Figure 5**).

Electrochemical impedance spectroscopy (EIS) is a useful technique to characterize interface reactions and electrode kinetics in HER. **Figure 6** showed the representative Nyquist and Bode plots of the EIS response of the MoS_2/MGF-modified GCE at various overpotentials. In the high frequencies zone, the MoS_2/MGF-modified electrode exhibited one capacitive semicircle, indicating that the corresponding equivalent circuit for the HER was characterized by one time constant and the reaction was kinetically controlled. The electrical equivalent circuit diagram given in **Figure 7**A was used to model the solid-liquid interface, and the experimental data were well fitted in Figure 7B,C, where a constant phase element (CPE) was employed. The impedance parameters by fitting the EIS responses are listed in Supporting Information, Table S1. The solution resistance R_s was overpotential independent about 9 Ω. The charge transfer resistance R_{ct} is related to the electrocatalysis kinetics and a lower value corresponds to a faster reaction rate. In this system, the values of R_{ct} decreased significantly with increasing overpotentials, from ≈1.81 kΩ at 90 mV to

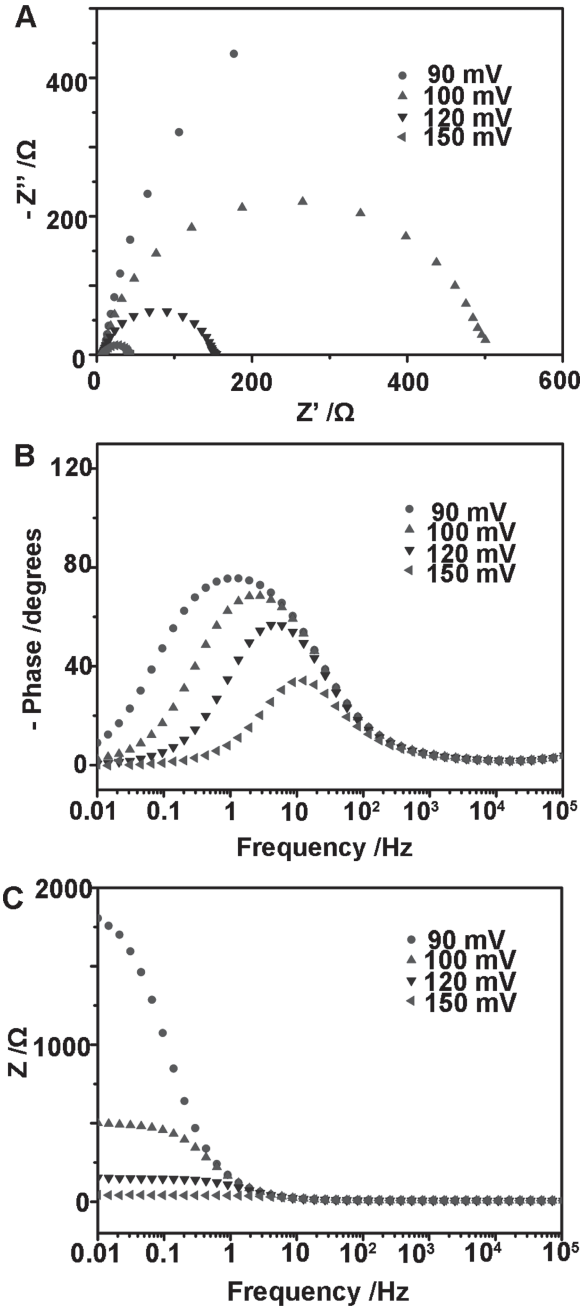

Figure 6. A) Nyquist and B,C) Bode plots showing EIS responses of MoS_2/MGF-modified glassy carbon electrode at various HER overpotentials in 0.5 m H_2SO_4.

only ≈33 Ω at 150 mV, respectively. The interfacial capacitance was slightly dependent on the overpotentials for MoS_2/MGF-modified electrode and CPE was ≈10.4 mF cm^{-2} at 100 mV. The high interfacial capacitance is due mainly to the specific surface area of mesoporous graphene so that it is nearly potential independent. The charge transfer resistance stems mainly from the MoS_2/MGF electrocatalyst and therefore varies with the applied overpotentials. Both lower charge-transfer resistance and higher interfacial capacitance illustrated the superior electrocatalytic activity of the MoS_2/MGF nanocomposites.

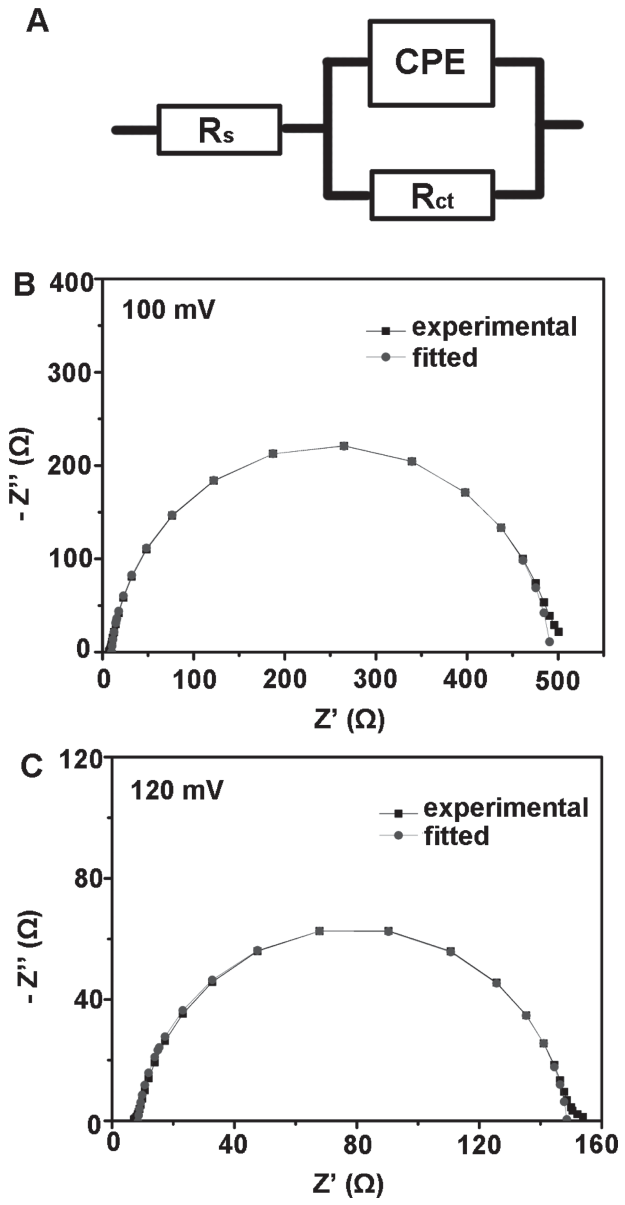

Figure 7. A) Equivalent electrical circuit used to model the HER process on MoS_2/MGF-modified GCE. Nyquist plots of MoS_2/MGF-modified GCE at overpotential of B) 100 mV and C) 120 mV. The square symbols were experimental data and lines with the dots were modeled by (A).

2.3. Mechanism of HER at the MoS_2/MGF-Modified GCE

According to the classic theory on the mechanism of hydrogen evolution, the overall HER reaction occuring at a MoS_2 modified electrode surface in acidic media (Equation 1) may theoretically proceed via a discharge step (Volmer-reaction, Equation 2) followed by either an ion and atom reaction (Heyrovsky-reaction, Equation 3) or combination reaction (Tafel-reaction, Equation 4),

$$2H_3O^+ + 2e^- \underset{k_-}{\overset{k}{\rightleftharpoons}} 2H_2O + H_2 \quad (1)$$

$$\text{Discharge reaction } H_3O^+ + M + e^- \underset{k_{V-}}{\overset{k_V}{\rightleftharpoons}} H_2O + M\text{-}H \quad (2)$$

$$\text{Ion and atom reaction } M\text{-}H + H_3O^+ + e^- \underset{k_{H-}}{\overset{k_H}{\rightleftharpoons}} H_2 + M + H_2O \quad (3)$$

$$\text{Combination reaction } 2M\text{-}H \underset{k_{T-}}{\overset{k_T}{\rightleftharpoons}} 2M + H_2 \quad (4)$$

where M denotes an active edge site of the catalyst and M-H denotes a hydrogen atom adsorbed at that edge site. Generally, the initial discharge step to form adsorbed hydrogen is considered to be fast, while the following hydrogen desorption step is typically rate-limiting.[28] Nørskov and co-workers calculated the fractional surface coverage of adsorbed hydrogen (θ) to be 0.25 on MoS_2 edge sites using density functional theory calculations of the hydrogen binding energy.[15,29] This supports an electrochemical desorption orientated Volmer-Heyrovsky mechanism (Equations 2,3), while the HER on a Pt surface is known to proceed through the Volmer-Tafel mechanism with a very high adsorbed hydrogen coverage ($\theta \approx 1$).[21]

We can determine which HER mechanism predominates for a specific electrode modification through a Tafel plot analysis of the obtained polarisation curves.[30] Herein, Tafel plots for MoS_2/MGF, MoS_2-MGF, and pure MoS_2 modified GCEs are shown in Figure 4A. Linear fittings have been carried out using the Tafel equation $h = a + b \log j$ to obtain Tafel slopes and values of the exchange current density (j_0) for each modified electrode. In principle, a lower Tafel slope means a catalyst requires a lower applied overpotential to generate a required current and j_0 is a measure of the electron transfer rate of the catalyst.[31] Caution must be taken when interpreting Tafel plots, however, as the Tafel slope varies in a complex manner depending on many factors (reaction pathway, catalyst preparation, catalyst categories, adsorption conditions of the active site, electrode modification procedure, etc.) and the full set of factors influencing the Tafel slope for MoS_2-derived catalysts are not yet fully elucidated.[16] In this work, we may tentatively assign a reaction mechanism for HER based on the obtained Tafel slopes but the main value of our data lies in qualitatively comparing our Tafel slopes with those for similarly modified electrodes in the literature.[5,6,13,19,21]

Thus, the Tafel slope for MoS_2/MGF-GCEs, determined at low overpotentials, h = 90–120 mV, was ≈42 mV decade^{-1} and the log j_0 was –2.52 log [mA cm^{-2}]. At larger overpotentials, h = 215–235 mV, the Tafel slope was ≈131 mV decade^{-1} and the log j_0 was –0.47 log [mA cm^{-2}]. The relatively low Tafel slope at low overpotentials is in line with MoS_2/graphene modified GCEs,[21] precatalyst amorphous MoS_x (x = 2, 3) films prepared by electropolymerization of $[MoS_4]^{2-}$ on FTO (fluorinated tin oxide) and GCEs[5,32] and precatalyst amorphous MoS_3 particles spray cast onto FTO and GCEs.[13] Indeed various Tafel slopes were reported in literature for MoS_2-related catalysts with different preparation routes. For instance, Tafel slopes of 57.6 and 60.1 mV decade^{-1} were obtained with a hybrid material of MoS_2/rGO synthesized by a microwave method reported by Leite and coworkers,[20] and the Tafel slope for MoS_2 crystals was 55–60 mV decade^{-1} reported by Chorkendorff and coworkers.[18] A common feature of each of the aforementioned catalysts is the enhanced quantity of unsaturated sulfur atoms

present at the surfaces of these sulfide materials, i.e. more catalytic edge sites are available per mole of deposited MoS_2. The Tafel slope for MoS_2/MGF-GCEs of 42 mV decade^{-1} suggests that the HER takes place via a rapid Volmer reaction (Equation 2) followed by a rate-limiting Heyrovsky step (Equation 3), according to the classical theory for HER in acidic media.[33–35] The theory outlining the basis of the Tafel slopes, at both low and high applied overpotentials, for a Volmer-Heyrovsky (rate determining step) mechanism of hydrogen evolution at MoS_2 catalytic edge sites is presented in Supporting Information, SI-A).

3. Conclusions

In conclusion, we have presented a highly active electrocatalyst of MoS_2/MGF where the MoS_2 nanoparticles were formed uniformly on mesoporous graphene foams via a facile solvothermal approach. MGF has a high surface area, abundant mesopores, and a highly conductive skeleton of graphene that provides a specific microenvironment and conductively multiplexed pathways to facilitate the rapid diffusion of ions and electrons. The MoS_2/MGF nanocomposites exhibited the higher HER activity with a low overpotential and large apparent cathodic currents. A small Tafel slope of ≈42 mV decade^{-1} suggested a Volmer-Heyrovsky mechanism for the catalyzed HER. These findings were attributed to an increased abundance of exposed catalytic edge sites and excellent electrical coupling to the underlying MGF modified electrode. MGF supported nano-MoS_2 is a highly active electrocatalyst, making it a potential matrix for cost-effective catalysts in electrochemical hydrogen production.

4. Experimental Section

Reagents: Pluronic F108, tetraethoxysilane (TEOS), dimethoxydimethylsilane (DMDMS), $(NH_4)_2MoS_4$ (99.97%), hydrazine monohydrate (98%), Nafion perfluorinated ion-exchange resin solution (5% w/w) and graphene oxide were purchased from Sigma-Aldrich. 1,3,5-trimethylbenzene (TMB), dimethylformamide (DMF, ≥99.5%), and ethanol were obtained from the Shanghai Chemical Plant.

Synthesis of MoS_2/MGF Nanocomposites: Mesoporous graphene foams (MGF) were prepared by using methyl group grafted silica nanospheres as the templates according to Zhao's method.[25] Graphene oxide sheets (GOs) were employed as the precursor for the construction of MGF. Due to the hydrophobic interaction between methyl group-grafted SiO_2 nanospheres and GOs, GOs could self-assemble outside SiO_2 to form lamellar-like structures. High temperature annealing was used to reduce graphene oxide to graphene. Briefly, Pluronic F108 (0.5 g) and 1,3,5-trimethylbenzene (TMB) (0.5 g) were mixed into a HCl solution (2 M, 15 mL) and kept stirring for 6 h at 25 °C. TEOS (0.5 g) was added drop-wise into this suspension under vigorous stirring. After 6 h, dimethoxydimethylsilane (DMDMS) (0.25 g) was added into the suspension and the reaction proceeded for another 24 h. Next, the mixture was dialyzed in distilled water for 48 h and the dialyzed suspension diluted to 30 mL by distilled water. Separately, graphene oxide (0.3 g) was dispersed into distilled water (300 mL) and sonicated for 2 h to form a homogeneous suspension. Subsequently, the two suspensions were mixed and left to stir for 12 h at room temperature. The resultant solid precipitate was collected by centrifugation at 4500 r min^{-1} and dried at 50 °C. The dried precipitate was calcinated at 900 °C for 5 h under an argon atmosphere. Finally, the sample was washed by HF (5%, 40 mL) twice to obtain the desired final product, MGF. For control experiments, non-porous graphene foams were prepared by using the same method from high temperature annealing at 900 °C but without methyl group-grafted SiO_2 nanospheres as the templates. MoS_2/MGF nanocomposites were prepared by a one-step hydrothermal method.[19,21] Typically, $(NH_4)_2MoS_4$ (22 mg) was added into DMF (10 mL) containing dispersed MGF (10 mg). The mixture was sonicated to obtain a homogeneous suspension, $N_2H_4{\cdot}H_2O$ (0.1 mL) was then added, followed by 30 min of further sonication. The suspension was transferred into a 40 mL Teflon-lined autoclave and heated in an oven at 200 °C for 12 h. The product was collected by centrifugation at 10 000 rpm for 3 min and washed with distilled water at least 5 times. The final product was obtained after lyophilization for 24 h. For comparison, MoS_2 nanoparticles formed on graphene or non-porous graphene were synthesized by the same process as MoS_2/MGF by simply replacing MGF with graphene oxide sheets or non-porous graphene foams from high temperature annealing, as above. MoS_2 nanoparticles formed on mesoporous carbon nanospheres were also prepared by the same process using MCNs as the matrices instead of MGF according to our previous work.[19] MCNs were synthesized by using triblock copolymer Pluronic F127 as a template and phenolic resol as a carbon source. The pure MoS_2 nanoparticles were synthesized using the same process in the absence of MGF.

Characterization: Scanning electron microscopy (SEM) images were recorded by a JEOL 6400 microscope operated at 10 keV. Transmission electron microscopy (TEM) studies were carried out using a JEOL JEM-2011 electron microscope at an acceleration voltage of 200 keV. X-ray photoelectron spectroscopic (XPS) analysis was performed on a Perkin-Elmer PHI 5000C spectrometer using Mg Kα radiation (1253.6 eV with pass energy of 20.0 eV). The carbonaceous C 1s line (284.6 eV) was used as the reference to calibrate the binding energies (BE). Nitrogen adsorption/desorption isotherms were collected with the aid of Quantachrome's Quadrasorb SI analyzer at 77 K. Prior to measurements, the samples were degassed at 523 K for 3 h under vacuum. The Brunauer-Emmett-Teller (BET) method was used to calculate the specific surface area. The pore size distribution was derived from the adsorption branch of the isotherms, using the BJH method with a spherical pore model. The total pore volume was calculated from the adsorbed amount at a maximum relative pressure P/P_0.

Electrochemical Measurements: The MoS_2/MGF hybrid catalyst (4 mg) was dispersed in a solution (1 mL) composed of 4:1 (v/v) distilled water and ethanol containing Nafion (80 μL, 5% wt) by sonication to form an homogeneous slurry. Then, an amount of the slurry was loaded onto the surface of a glassy carbon electrode (GCE, 3.5 mm in diameter) with a hybrid catalyst loading of 0.21 mg cm^{-2}. The modified MoS_2/MGF-GCE was left to dry at room temperature. For comparison, GCEs were also modified with pure MoS_2, pure MGF, a physical mixture of MoS_2 and MGF (MoS_2-MGF), MoS_2-loaded on graphene sheets, MoS_2-loaded on non-porous graphene and MoS_2-loaded on mesoporous carbons. Each modified GCE was loaded with the same amount of MoS_2. All electrochemical studies were performed using a CHI660C potentiostat (CH Instruments, Texas, USA) in a standard three-electrode setup with a modified glassy carbon working electrode, saturated calomel electrode (SCE) as the reference, and platinum foil as a counter electrode. Prior to measurement, a resistance test was made and the *iR* compensation was applied using the CHI software. The electrocatalytic activity of MoS_2/MGF towards the HER was examined by polarization curves using linear sweep voltammetry (LSV) at a scan rate of 2 mV s^{-1} in 0.5 m H_2SO_4 at room temperature. Electrochemical impedance spectroscopic (EIS) measurements were carried out by an AutoLab in 0.5 m H_2SO_4 at various overpotentilas from 90 mV to 150 mV (vs. RHE) in the frequency range 10^{-2} to 10^6 Hz with a single modulated AC potential of 10 mV. Experimental EIS data were analysed and fitted with the software NOVA 1.7.

Supporting Information

Supporting Information is available from the Wiley Online Library or from the author.

Acknowledgements

This work was supported by NSFC 20925517 and SKLEAC201101. We would like to thank the Swiss Science Foundation grant "Solar Fuels" 200 021-134 745.

Received: January 26, 2013
Revised: March 13, 2013
Published online: May 22, 2013

[1] J. A. Turner, *Science* **2004**, *305*, 972.
[2] N. S. Lewis, D. G. Nocera, *Proc. Natl. Acad. Sci. USA* **2006**, *103*, 15729.
[3] M. S. Dresselhaus, I. L. Thomas, *Nature* **2001**, *414*, 332.
[4] M. G. Walter, E. L. Warren, J. R. McKone, S. W. Boettcher, Q. Mi, E. A. Santori, N. S. Lewis, *Chem. Rev.* **2010**, *110*, 6446.
[5] D. Merki, H. Vrubel, L. Rovelli, S. Fierro, X. Hu, *Chem. Sci.* **2012**, *3*, 2515.
[6] P. Ge, M. D. Scanlon, P. Peljo, X. Bian, H. Vubrel, A. O'Neill, J. N. Coleman, M. Cantoni, X. Hu, K. Kontturi, B. Liu, H. H. Girault, *Chem. Commun.* **2012**, *48*, 6484.
[7] D. E. Bartak, B. Kazee, K. Shimazu, T. Kuwana, *Anal. Chem.* **1986**, *58*, 2756.
[8] P. Millet, F. Andolfatto, R. Durand, *Int. J. Hydrogen Energy* **1996**, *21*, 87.
[9] H. B. Gray, *Nat. Chem.* **2009**, *1*, 7.
[10] M. R. DuBois, D. L. DuBois, *Chem. Soc. Rev.* **2009**, *38*, 62.
[11] A. M. Appel, D. L. DuBois, M. R. DuBois, *J. Am. Chem. Soc.* **2005**, *127*, 12717.
[12] T. B. Rauchfuss, *Inorg. Chem.* **2004**, *43*, 14.
[13] H. Vrubel, D. Merki, X. Hu, *Energy Environ. Sci.* **2012**, *5*, 6136.
[14] J. D. Benck, Z. Chen, L. Y. Kuritzky, A. J. Forman, T. F. Jaramillo, *ACS Catal.* **2012**, *2*, 1916.
[15] B. Hinnemann, P. G. Moses, J. Bonde, K. P. Jørgensen, J. H. Nielsen, S. Horch, I. Chorkendorff, J. K. Nørskov, *J. Am. Chem. Soc.* **2005**, *127*, 5308.
[16] A. B. Laursen, S. Kegnæs, S. Dahl, I. Chorkendorff, *Energy Environ. Sci.* **2012**, *5*, 5577.
[17] J. Bonde, P. G. Moses, T. F. Jaramillo, J. K. Nørskov, I. Chorkendorff, *Far. Discuss.* **2008**, *140*, 219.
[18] T. F. Jaramillo, K. P. Jorgensen, J. Bonde, J. H. Nielsen, S. Horch, I. Chorkendorff, *Science* **2007**, *317*, 100.
[19] X. Bian, J. Zhu, L. Liao, M. D. Scanlon, P. Ge, C. Ji, H. H. Girault, B. Liu, *Electrochem. Commun.* **2012**, *22*, 128.
[20] E. G. S. Firmiano, M. A. L. Cordeiro, A. C. Rabelo, C. J. Dalmaschio, A. N. Pinheiro, E. C. Pereira, E. R. Leite, *Chem. Commun.* **2012**, *48*, 7687.
[21] Y. Li, H. Wang, L. Xie, Y. Liang, G. Hong, H. Dai, *J. Am. Chem. Soc.* **2011**, *133*, 7296.
[22] S. Zhu, S. Tang, J. Zhang, B. Yang, *Chem. Commun.* **2012**, *48*, 4527.
[23] Q. He, S. Wu, Z. Yin, H. Zhang, *Chem. Sci.* **2012**, *3*, 1764.
[24] Q. Chen, L. Zhang, G. Chen, *Anal. Chem.* **2012**, *84*, 171.
[25] X. Huang, K. Qian, J. Yang, J. Zhang, L. Li, C. Yu, D. Zhao, *Adv. Mater.* **2012**, *24*, 4419.
[26] C. Li, G. Shi, *Nanoscale* **2012**, *4*, 5549.
[27] X.-C. Dong, H. Xu, X.-W. Wang, Y.-X. Huang, M. B. Chan-Park, H. Zhang, L.-H. Wang, W. Huang, P. Chen, *ACS Nano* **2012**, *6*, 3206.
[28] J. Zhu, J. Tang, L. Zhao, X. Zhou, Y. Wang, C. Yu, *Small* **2010**, *6*, 276.
[29] E. Sku´lason, G. S. Karlberg, J. Rossmeisl, T. Bligaard, J. Greeley, H. Jo´nsson, J. K. Nørskov, *Phys. Chem. Chem. Phys.* **2007**, *9*, 3241.
[30] S. Fletcher, *J. Solid State Electrochem.* **2008**, *13*, 537.
[31] P. Atkins, J. D. Paula, *Atkins' Physical Chemistry*, 7th Ed. Oxford University, UK, **2002**.
[32] D. Merki, X. Hu, *Energy Environ. Sci.* **2011**, *4*, 3878.
[33] J. O. M. Bockris, E. C. POTTER, *J. Electrochem. Soc.* **1952**, *99*, 169.
[34] J. O. M. Bockris, S. U. M. Khan, *Surface Electrochemistry: A Molecular Level Approach*, Plenum, New York **1993**.
[35] B. E. Conway, B. V. Tilak, *Electrochim. Acta* **2002**, *47*, 3571.